Indones. J. Chem., xxxx, xx (x), xx - xx

1

Preparation, Structural Identification and Biomedical Evaluation of Some New Complexes

Alyaa Khider Abbas[1]* and Asmaa Edrees Fadhil[2]

[1]Department of Chemistry, College of Science, University of Baghdad, Al Jadriya Street, Baghdad 10071, Iraq

[2]College of Pharmacy, Al-Turath University, Al Mansour Street, Baghdad 10013, Iraq

Abstract: *A new nano azo ligand, [2-amino-6-oxo-6,7-dihydro-1H-purin-8-yl)diazenyl)nitrobenzene (AH), and its Ag(I), Cu(II), and Zn(II) complexes were successfully synthesized and characterized using elemental analyses, magnetic susceptibility, molar conductance, and spectroscopic techniques (FTIR, UV-vis, ¹H-NMR), along with thermal analysis. FTIR confirmed the ligand acts as a neutral* N,N-*bidentate. The metal-to-ligand ratio was determined to be 1:1 for Ag(I) and Zn(II) complexes and 1:2 for the Cu(II) complex. Stability constants and Gibbs free energy, assessed via spectrophotometry, indicated high stability for all complexes. SEM and X-ray diffraction revealed nanoscopic properties for the Ag(I) and Cu(II) complexes. The antimicrobial activity against* Staphylococcus aureus, Klebsiella pneumoniae, *and* Candida albicans *species showed good efficiency compared to reference drugs. The ligand also exhibited moderate antioxidant activity using the DPPH assay. Additionally, the Zn(II) complex demonstrated effective anti-inflammatory activity, promoting wound healing within 14 days, compared to 16 days with silver sulfadiazine and 18 days without treatment.*

Keywords: *hypoxanthine-azo ligand; anti-microbial activity; antioxidant; burn healing*

■ INTRODUCTION

Azo dyes, constituting approximately for more than half of all commercial dyes and colorants, are recognized as the most significant class of dyes. They are used for extensive applications across various scientific and technological fields [1-2]. The ease of performing diazotization and azo coupling reactions has led to extensive research on azo dyes compared to other dye classes [3]. Research has also focused on azo dyes containing heterocyclic rings due to their outstanding qualities. These dyes serve as efficient coloring agents in numerous textile applications. The use of heterocyclic rings as coupling components has enabled the development of colorants with strong chromophores, vibrant colors, and high levels of dyeing and fastness properties [4].

Synthetic azo compounds have been shown to exhibit antifungal, anticancer, and antibacterial activities while maintaining low toxicity to healthy cells. Their minimal toxicity, including reduced risks of allergic and hyperactive reactions, has led to their frequent use in food, medicine, paint, polymers, and other products. Numerous investigations on the synthesis and conformational characteristics of azo compounds have been reported in recent years [5-7].

Hypoxanthine, a purine derivative, has long been recognized as a pivotal molecule in various cellular processes [8-9]. Although it is relatively less abundant compared to other purine metabolites, emerging research has illuminated its multifaceted roles in cellular metabolism, signaling pathways, and disease pathogenesis. This provides a comprehensive exploration of hypoxanthine's metabolism, physiological functions, and implications for health and disease. Additionally, potential therapeutic strategies targeting hypoxanthine metabolism for the treatment of various disorders are discussed.

Purine metabolism is a highly regulated biochemical pathway crucial for cellular function and

homeostasis. As an intermediate metabolite in this pathway, hypoxanthine plays essential roles in nucleotide synthesis, energy metabolism, and signaling cascades. Historically overshadowed by its counterpart's adenine and guanine, the significance of hypoxanthine in diverse physiological processes and pathological conditions has become increasingly evident [10]. In this work, the primary objective is to prepare new complexes of Ag(I), Cu(II), and Zn(II) from the ligand (AH) and to identify them using various physicochemical methods. The complexes were analyzed based on spectral methods, thermal analyses, and other analytical techniques, and their antimicrobial, antioxidant, and anti-inflammatory activities were screened.

■ EXPERIMENTAL SECTION

Materials

The materials were utilized from Sigma-Aldrich with analytical grade without further purification. In this study, several chemicals were used, such as *p*-nitroaniline (99%), hypoxanthine (99%), $CuCl_2·2H_2O$ (99%), silver nitrate (99%), and zinc chloride (98%). Several microorganisms were used in this study, such as *Staphylococcus aureus* (ATCC 25923), *Klebsiella pneumonia* (ATCC 13883), and *Candida albicans* (ATCC 14053).

Instrumentation

Elemental analysis for C, H, and N in AH and its complexes was conducted using an Euro EA 3000 Elemental Analyzer, while the metal content was determined by AAS with a Nova 350.0 spectrophotometer. Infrared spectra (400–4000 cm^{-1}) were recorded using a Shimadzu 8400s spectrophotometer with KBr pellets. UV-vis spectra were measured on a Shimadzu 1800 UV-vis spectrophotometer. ^{1}H-NMR spectra were obtained using a BRUKER AV 400 Avance-III (400 and 100 MHz). Thermogravimetric analysis (TGA) was performed on an SDT Q600 V20.9 Build, and melting points were measured using a Gallenkamp melting point apparatus. Chloride concentrations in the complexes, whether counter-ion or coordinated, were determined by the Mohr method. Magnetic susceptibilities were measured at ambient temperatures using a Sherwood Scientific Auto Magnetic Susceptibility Balance. Finally, molar conductance of the synthesized complexes was evaluated with a HI9811-5 Hanna instrument.

Procedure

Synthesis of AH ligand

The AH ligand was prepared using a general procedure as previously notified [3]. The *p*-nitroaniline (1.38 g; 0.01 mol) was used to prepare diazonium salt, while 1.36 g or 0.01 mol of hypoxanthine was used as coupling reagent. Scheme 1 represents the new AH ligand preparation process.
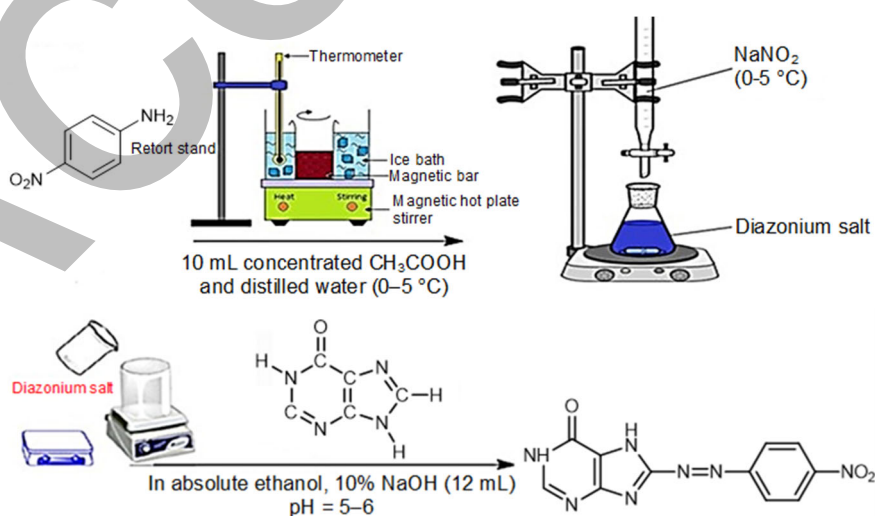
Scheme 1. Proposed route for ligand synthesis

Indones. J. Chem., xxxx, xx (x), xx - xx

3

Preparation of new metal ion complexes

Cu(II) complex was synthesized in a molar ratio of 1:2. In contrast, Ag(I) and Zn(II) complexes were synthesized in a mol ratio of 1:1. The synthesizing path was depicted in Scheme 2, and the reaction was followed by TLC using a mixture solvent of ammonia:butanol:methanol of 1.5:1:1. Table 1 shows some physical and chemical features.

Antimicrobial test

The antimicrobial effectiveness was evaluated using the minimum inhibitory concentration (MIC) method [7] against Gram-positive bacteria (*S. aureus*), Gram-negative bacteria (*K. pneumoniae*), and fungi (*C. albicans*), with deionized distilled water as the solvent. Amoxicillin and fluconazole were used as control agents. The microorganisms were cultured on nutrient agar medium, and the disc diffusion method was employed to assess the biological inhibitory activity of the ligand and its complexes. A 5 mL of the ligand and its complexes (1×10^{-3} M) were applied to the discs, which were incubated at 37 °C for 24 h, following a 15-min pre-incubation period to allow for diffusion in the bacterial culture. The inhibition zones were measured using a standardized scale to determine the antimicrobial activity.

Anti-inflammatory analysis

To evaluate the burn healing efficacy of [Zn(AH)Cl$_2$]·H$_2$O, three groups of male albino mice (*Mus musculus*) were used. At the start of the experiment, the mice were 8 to 10 weeks old, with weights ranging from 23 to 27 g. Each group was housed separately under controlled room temperature, with unrestricted access to water and standard pellet food. Hair removal was performed using Veet, a depilatory lotion, and burns were induced on the mice's skin using a flame. Recovery time was assessed based on the number of days required for the burn wounds to heal. The mice received treatment three times daily, with [Zn(AH)Cl$_2$]·H$_2$O as the test compound, silver sulfadiazine as a control, and an untreated group serving as a negative control [4].
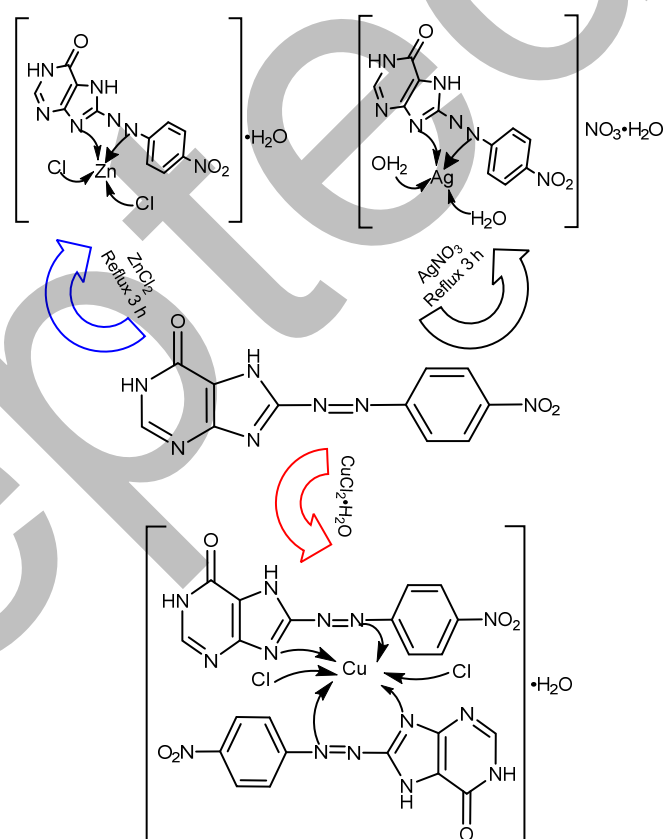
Scheme 2. Proposed route for ligand AH synthesis

Table 1. Physical features and elemental analysis

No	Compounds M.wt. (g/mol)	Color λ_{max} (nm)	M:L ratio	Λ_m (S cm^2/mol)	%Experimental (%Theoretical)				
					C	H	N	M	Cl
1	AH	Yellow	-	-	46.82	3.00	34.74	-	-
	285.00	420			(46.31)	(2.45)	(34.38)		
2	[Ag(AH)(H$_2$O)$_2$]NO$_3$·2H$_2$O	Orange	1:1	80.1	25.88	2.92	21.72	20.90	-
	526.86	480			(25.05)	(2.84)	(21.25)	(20.47)	
3	[Cu(AH)$_2$Cl$_2$]·H$_2$O	Green	1:2	37.3	36.87	2.44	27.94	8.45	9.41
	722.08	620			(36.53)	(2.21)	(27.12)	(8.79)	(9.82)
4	[Zn(AH)Cl$_2$]·H$_2$O	Pink	1:1	26.7	30.70	2.23	22.61	15.15	16.75
	439.65	510			(30.04)	(2.04)	(2.30)	(14.88)	(16.15)

Alyaa Khider Abbas and Asmaa Edrees Fadhil

Antioxidant effectiveness

The antioxidant activity of the ligand and the standard (vitamin C) was evaluated using the radical scavenging action of a stable DPPH free radical [4]. A 0.1 mL aliquot of either the extract or the standard (at concentrations of 12.5, 25, 50, 100, and 200 mg/mL) was mixed with 3.9 mL of DPPH solution. The mixtures were incubated for 30 min at 37 °C and the absorbance was measured at 517 nm. All measurements were done in triplicate. The radical scavenging ability was calculated using Eq. (1).

DPPH radical scavenging activity (%)

$$= \left(1 - \frac{\text{absorbance of sample}}{\text{absorbance of standard}}\right) \times 100\% \qquad (1)$$

■ RESULTS AND DISCUSSION

Scheme 1 illustrates the synthetic pathway for the novel azo-hypoxanthine (AH) ligand. The synthesis starts with the diazotization of a primary aromatic amine (*p*-nitroaniline) at 0–5 °C, resulting in the formation of a diazonium salt intermediate. This temperature range is maintained to prevent the decomposition and potential explosion of the diazonium salt at higher temperatures. The intermediate is then used immediately [5-6]. The diazonium salt is subsequently coupled with hypoxanthine, which acts as a nucleophile, in an ethanolic alkaline solution. The alkaline medium is used to increase nucleophilicity and prevent dissociation [11]. In this process, the diazonium salt functions as the electrophile. The synthesis is completed in a single step, with high yields and a short reaction time.

Additionally, nitrogen atoms, including an azo moiety with a pair of electrons, are considered binding sites for coordination with metal ions. The presence of donor atoms, such as N atom in hypoxanthine, which is located ortho to the azo moiety, provides additional coordination sites [3,7]. As a result, the ligand is regarded as a non-ionic *N,N*-bidentate ligand when interacting with Ag(I), Cu(II), and Zn(II) ions. The AH and its metal ion complexes are stable, non-hygroscopic solids with good storage properties. All complexes are non-electrolytes, except for the Ag-AH complex (1:1), which is an electrolyte with nitrate as the counterion and is soluble in water. All analytical data for the synthesized compounds correspond proportionally to their expected values. The compounds were formulated based on elemental analysis, FTIR, UV-vis, ^{1}H-NMR, thermal analysis, melting points, and magnetic susceptibility data.

Stoichiometry, Stability Constant, and Gibbs Free Energy

The mol ratio approach, a widely used method for determining the composition of a complex in solution, was employed [12]. This procedure is depicted in Fig. 1, and it was applied to obtain the results. The outcome indicates the formation of a 1:1 mol ratio for all synthesized complexes, except for the Cu-AH complex, which exhibits a 1:2 ratio.

The stability constant can be defined spectrophotometrically [4] by Eq. (2) and (3). This method was employed to estimate the stability constant for the Cu(II) complex with a 1:2 (M:L) ratio.

$$K = \frac{1 - \alpha}{4\alpha^3 C^2} \qquad (2)$$

$$\alpha = \frac{A_m - A_s}{A_m} \qquad (3)$$

In the context of determining the stability constant, α represents the degree of dissociation, A_s denotes the absorption of a solution with a stoichiometric 1:1 (M:L) ratio, A_m indicates the absorption of a solution containing an excess of ligands, and C refers to the concentrations of the synthetic solution (M).
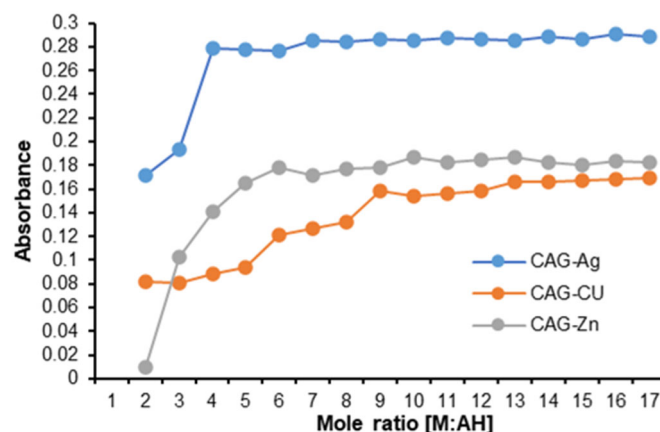

Fig 1. AH ligand and its complexes' mol ratio

Alyaa Khider Abbas and Asmaa Edrees Fadhil

For Ag(I) and Zn(II) complexes with 1:1 (M:L) ratio, the stability constant can be computed using Eq. (4).

$$K = \frac{1 - \alpha}{\alpha^2 C} \qquad (4)$$

The results are shown in Table 2, where the stability of the complexes increases in the following order: [Cu(AH)$_2$Cl$_2$]·H$_2$O < [Ag(AH)(H$_2$O)$_2$]NO$_3$·2H$_2$O < [Zn(AH)Cl$_2$]·H$_2$O. The thermodynamic coefficient, Gibbs free energy (ΔG), was calculated using the following Eq. (5) [13];

$$\Delta G = -RT \ln K \qquad (5)$$

where R is the gas constant (8.31 J/mol K) and T represents temperature (K). From the ΔG data, it was determined that all synthesized complexes form spontaneously.

Thermogravimetric Analysis

The thermal analysis data of the ligand and its metal complexes provide insights into the decomposition of the ligand, metal oxides, and several water molecules [14].

The analysis was conducted from room temperature to 800 °C under argon gas, as illustrated in Fig. S1(a-d), and summarized in Table 3. The TGA curve of the ligand exhibited 4 primary decomposition steps within the temperature ranges of 25–48, 48–300, 300–575, and 575–800 °C, with mass losses of 2.12%, 26.79%, 25.62%, and 9.97%, respectively, for the AH ligand. The TGA of the complexes displayed 5 sequential steps. The initial step in all complexes involved the loss of lattice water in the 25–80 °C range. Subsequent steps were associated with the release of chloride ions, ligand molecules, and nitrate ions, while decomposition concluded with the formation of metal oxides as the final residue [15-17].

FTIR Spectroscopy

The identity of the ligand was determined by comparing its FTIR spectrum with those of the synthesized metal ion complexes. The significant bands for AH and its metal ion complexes are summarized in

Table 2. K, ln K, and ΔG of AH complexes

Complex	A_s	A_m	α	K	ln K	ΔG (kJ/mol)
[Ag(AH)(H$_2$O)$_2$]NO$_3$·2H$_2$O	0.280	0.291	0.037	7.03×10^7	13.46	−30,544.21
[Cu(AH)$_2$Cl$_2$]·H$_2$O	0.090	0.169	0.467	1.30×10^7	14.08	−31,945.33
[Zn(AH)Cl$_2$]·H$_2$O	0.163	0.178	0.084	1.29×10^5	11.77	−26,713.08

Table 3. The thermogravimetric analyses of the ligand and its complexes

Compound (Molecular formula)	Stage	Extent of thermal decomposition (°C)	Proposed part	%mass loss	
				Calculated	Found
AH (C$_{11}$H$_7$N$_7$O$_3$)	1	25–48	H$_3$C$_{0.25}$	2.10	2.12
	2	50–300	H$_2$C$_6$	26.66	26.79
	3	300–575	C$_{4.75}$N	24.91	25.62
	4	575–800	N$_2$	9.82	9.97
	Residue	> 800	N$_4$O$_3$	36.49	35.52
[Ag(AH)(H$_2$O)$_2$]NO$_3$·2H$_2$O (AgC$_{11}$H$_{15}$N$_8$O$_{10}$)	1	25–80	H$_2$O	3.41	2.87
	2	80–400	H$_2$O·C$_3$H$_6$	11.38	11.78
	3	400–500	C$_5$H$_3$	11.95	12.80
	4	500–675	C$_3$H$_3$N$_{7.5}$	27.14	27.39
	5	675v800	N$_{0.7}$O$_3$	10.43	10.04
	Residue	> 800	AgO$_5$	35.49	35.09
[Cu(AH)$_2$Cl$_2$]·H$_2$O (CuC$_{22}$H$_{16}$N$_{14}$O$_7$Cl$_2$)	1	25–50	H$_2$O$_{0.25}$	0.83	0.95
	2	40–275	Cl$_{1.35}$O$_{0.75}$	8.29	8.44
	3	275–490	C$_{6.5}$H$_{14}$Cl$_{0.65}$	15.91	16.41
	4	490–698	C$_{15.5}$N$_3$	31.55	31.39
	5	698–800	N$_{7.5}$	14.53	14.79
	Residue	> 800	CuN$_{3.5}$O$_6$	28.86	28.05

Compound (Molecular formula)	Stage	Extent of thermal decomposition (°C)	Proposed part	%mass loss Calculated	Found
	1	25–55	$H_2O_{0.5}$	2.27	1.43
	2	55–84	$Cl_2O_{0.5}$	17.97	17.63
$[Zn(AH)Cl_2] \cdot H_2O$	3	84–560	$C_{6.5}H_7$	19.34	18.84
$(ZnC_{12}H_9N_7O_4Cl_2)$	4	560–698	$C_{4.5}N_{1.3}$	16.40	16.73
	5	698–800	$N_{4.2}$	13.38	13.83
	Residue	> 800	$ZnN_{1.5}O_3$	30.58	31.54

Table 4. In the spectrum of the ligand, two bands at 1616 and 1568 cm^{-1}, attributed to $\nu(C=N)$ in the imidazole ring of hypoxanthine, were altered in position and shape in the spectra of all complexes due to coordination with the metal ions [18-20]. The $\nu(N–H)$ and $\nu(C=O)$ bands in the free AH ligand spectrum remained unchanged in the spectra of all complexes, indicating that these moieties did not participate in the chelating ring. Minor changes in the position or form of these bands were occasionally observed, which were associated with variations in resonance due to chelation [7,21].

Notable bands for the azo compound, namely $\nu(N=N)$ and $\nu(C–N=N–C)$, appeared at 1473 and 1375 cm^{-1} in the AH spectrum, respectively. The position and intensity of these bands were diminished in the spectra of the complexes, suggesting that the nitrogen of the azo moiety is involved in coordination [22-24]. New bands in the ranges 501–514, 603–605, 659, and 418–420 cm^{-1}, were observed, which may correspond to $\nu(M–N_{azo})$, $\nu(M–N_{imd})$, and $\nu(M–Cl)$, respectively. Additionally, a new band at 540 cm^{-1} in the Ag-complex spectrum is attributed to $\nu(M–O_{water})$. These observations support the conclusion that the ligand acts as a neutral *N,N*-bidentate ligand, forming a penta-chelating ring [25-27].

Electronic Spectra and Magnetic Amusement Data

The electronic spectrum of the ligand in absolute ethanol (10^{-4} M) within the range of 280–1100 nm is depicted in Fig. S2(a). Two bands are observed: the first band appears at 295 nm (33,898 cm^{-1}), corresponding to the $\pi \rightarrow \pi^*$ intramolecular transition of heterocyclic and aromatic moieties [28]. The second band, observed at 420 nm (23,809 cm^{-1}), is attributed to the $n \rightarrow \pi^*$ transition of the intramolecular charge transfer involving the carbonyl, nitro, and azo moieties [29-30].

The electronic spectra of the diamagnetic d^{10} of Ag(I) and Zn(II) complexes reveal a sharp absorption band, as shown in Fig. S2(b) and (c), and summarized in Table 5. This band is assigned to charge transfer (CT) [7,31]. The electronic spectrum of the $[Cu(AH)_2Cl_2] \cdot H_2O$ complex, shown in Fig. S2(d), displays two bands at 925 (10,810 cm^{-1}) and 780 nm (12,820 cm^{-1}). These bands are assignable to the $(2B_1g \rightarrow 2A_1g)$ (ν_1) and $(2B_1g \rightarrow 2B_2g)$ (ν_2) transitions, respectively. The ν_3 transition $(2B_1g \rightarrow 2E_1g)$ is obscured by the charge transfer band at 620 nm (16,129 cm^{-1}) [32-33], which is characteristic of a distorted octahedral geometry with Jahn-Teller distortion (D_4h). The magnetic moment is measured as μ_{eff} = 1.33 B.M.

Table 4. FTIR spectral vibration of the free ligand and its complexes

Compound	$\nu(OH)$	$\nu(NH_2)$	$\nu(C=O)_{py}$	$\nu(C=N)_{imd}$	$\nu(N=N)$	$\nu(-CN=N-C-)$	$\nu(M-N)_{imd}$	$\nu(M-N)_{azo}$	$\nu(M-Cl)$	$\nu(M-O_{water})$
AH	3332	3174–3114	1695–1672	1616–1568	1473	1375	-	-	-	-
	s	d, sh	d, sh	d, sh	sh	sh				
$[Ag(AH)(H_2O)_2]NO_3 \cdot 2H_2O$	3342	3114	1693–1672	1631–1564	1375	1263	603	501	-	540
	m	d	d	d, w	m	w	w	w		w
$[Cu(AH)_2Cl_2] \cdot H_2O$	3423–3342	3186–3145	1706–1664	1606–1544	1382	1255	605	514	420	-
	d, s	d, s	d, s	d, w	s	m	m	w	vw	
$[Zn(AH)Cl_2] \cdot H_2O$	3419–3342	3172–3114	1693–1672	1631–1564	1415–1375	1263	605	503	418	-
	d, m	d, m	d, s	d, w	d, s	m	w	vw	vw	

*w: weak, sh: sharp, br: broad, s: strong, t: triple, py: pyrimidine, m: medium, d: double, and imd: imidazole

Alyaa Khider Abbas and Asmaa Edrees Fadhil

Table 5. The data of electronic spectra of AH ligand and its complexes

Compound	λ (nm)	Wavenumber (cm^{-1})	Assignment	Hybridization	Geometry
AH	295	33898	n→π*	-	-
	420	23809	n→π*	-	-
[Ag(AH)(H$_2$O)$_2$]NO$_3$·2H$_2$O	480	20833	CT	sp^3	Tetrahedral
[Cu(AH)$_2$Cl$_2$]·H$_2$O	925	10810	2B$_{1g}$→2A$_{1g}$		
	780	12820	B$_{1g}$→2B$_{2g}$	sp^{3}d^2	Distorted octahedral
	620	16129	CT		
[Zn(AH)Cl$_2$]·H$_2$O	510	19607	CT	sp^3	Tetrahedral

The ¹H-NMR Spectrum of AH Ligand

The ¹H-NMR analyses were found to corroborate the results from the FTIR spectrum. Chemical shifts (δ) in ppm for various types of protons in the ligand were observed, as shown in Fig. S3. A singlet signal was noted for the NH protons of the imidazole and pyrimidine moieties at 12.5 (1H) and 9 ppm (1H), respectively. Additionally, the aromatic ring displayed multiple signals at 7–8 ppm (4H) [3,34-36]. The ¹H-NMR spectrum was obtained in a DMSO-d_6 solution at 2.5 ppm [14].

XRD Analysis

Fig. 2 depicts the XRD patterns of AH and [Zn(AH)Cl$_2$]·H$_2$O in the range of 5–80°. The degree of crystallinity of these compounds was investigated using an X-ray source (Cu Kα). The most significant reflection peaks for the AH ligand and [Zn(AH)Cl$_2$]·H$_2$O are observed between 27.78–11.29 and 29.95–17.19°, respectively. The primary reflection peak for AH is located at 29.95°, while the corresponding peak for [Zn(AH)Cl$_2$]·H$_2$O is at 11.29°. The semi-crystalline nature and particle size of the AH ligand and [Zn(AH)Cl$_2$]·H$_2$O were estimated from the XRD patterns by employing the well-known Debye-Scherrer equation in Eq. (6) [37];

$$D = \frac{K\lambda}{\beta\cos\theta} \tag{6}$$

where D is the particle size (nm), β is the full width at half maximum (FWHM) of the X-ray diffraction peak, θ is the Bragg angle, λ is the X-ray wavelength (0.15406 nm), and K is a constant (0.9). The particle sizes for the AH ligand and [Zn(AH)Cl$_2$]·H$_2$O were calculated to be 4.15 and 1.844 nm, respectively (Table 6), indicating that both are within the nano-scale range.

The interplanar spacing (*d*) was calculated from the intense peak positions using Bragg's equation in Eq. (7) [38];

$$n\lambda = 2d\sin\theta \tag{7}$$

where λ = 1.5406 Å and n is an integer. The calculated and observed d values for the AH ligand are 2.9810 and 2.9807 Å, while for [Zn(AH)Cl$_2$]·H$_2$O, the values are 3.2095 and 3.2083 Å, respectively [39-40].
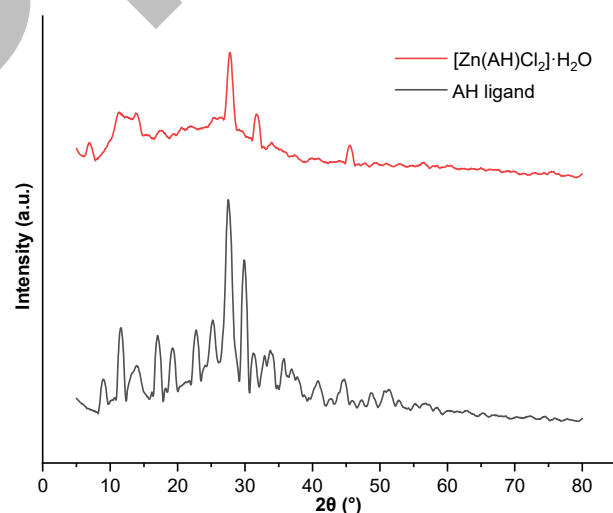
Fig 2. XRD for the AH ligand and [Zn(AH)Cl$_2$]·H$_2$O complex

Table 6. Particle size of ligand AH and [Zn(AH) Cl$_2$]·H$_2$O

Compounds	2θ	FWHM	D (nm)	d calculated (Å)	d found (Å)
AH ligand	29.95	0.2843	4.915	2.9810	2.9807
[Zn(AH)Cl$_2$]·H$_2$O	27.78	0.7550	1.844	3.2095	3.2083

SEM Analysis

An electron microscope known as an SEM generates a beam of electrons that interacts with the atoms in the sample, producing a range of signals. Some of these signals provide information about the sample's surface topography and composition. The surface homogeneities and crystalline structures of the ligand and its complexes were examined using SEM with a cross-sectional area of 100 nm and an enlargement power of 60,000×. The SEM images revealed heterogeneous surfaces with varying forms among different compounds and changes in particle volume (Fig. 3 and Table 7). The SEM technique demonstrated that both the ligand and its complexes possess nanoscale properties, with particle sizes in the nanometer range [19,25,41].

Study of Antibacterial and Antifungal Activity

Microbes are the primary cause of most diseases, making it crucial to find effective cures and inhibit their growth. Remedies for microbial infections are derived

Table 7. SEM technique for AH ligand and its complexes

Compound	Average volume (nm)	Shape
AH ligand	45.75	Coral
[Ag(AH)(H$_2$O)$_2$]NO$_3$·2H$_2$O	52.67	Coral
[Cu(AH)$_2$Cl$_2$]·H$_2$O	53.83	Coral
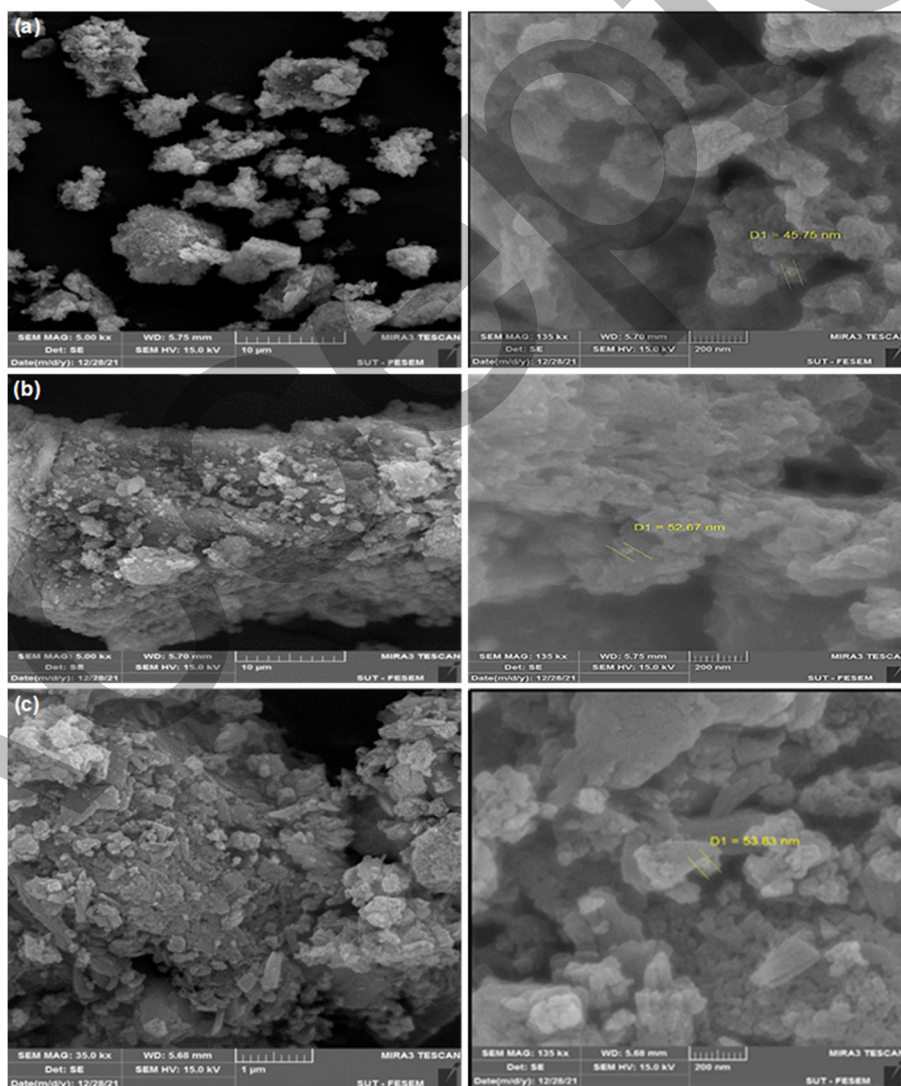
Fig 3. SEM results for (a) AH ligand, (b) [Ag(AH)(H$_2$O)$_2$]NO$_3$·2H$_2$O, and (c) [Cu(AH)$_2$Cl$_2$]·H$_2$O

from two main sources: natural products, such as penicillin obtained from the *Penicillium* fungus, and synthetic chemical compounds. Azo compounds and hypoxanthine are well-known for their potent antibacterial and antifungal properties. In many cases, the activity of metal complexes surpasses that of the ligands alone [42-46]. Hypoxanthine, in particular, has demonstrated remarkable pharmacological characteristics.

The current investigation revealed varying deactivation capacities of the tested compounds against selected bacteria and *C. albicans*. According to the findings summarized in Table 8, the antibacterial activity for *S. aureus* followed the order: $[Ag(AH)(H_2O)_2]NO_3 \cdot 2H_2O$ > $[Cu(AH)_2Cl_2] \cdot H_2O$ > $[Zn(AH)Cl_2] \cdot H_2O$ > AH. For *K. pneumoniae*, the order was: $[Cu(AH)_2Cl_2] \cdot H_2O$ > $[Zn(AH)Cl_2] \cdot H_2O$ > AH > $[Ag(AH)(H_2O)_2]NO_3 \cdot 2H_2O$. Against *C. albicans*, the activity was: $[Ag(AH)(H_2O)_2]NO_3 \cdot 2H_2O$ > $[Cu(AH)_2Cl_2] \cdot H_2O$ > $[Zn(AH)Cl_2] \cdot H_2O$ > AH.

The metal complexes exhibited greater activity and sensitivity against both bacteria and fungi compared to the free ligands. The mechanism of action for metal chelates can be explained by the chelation theory and the overtones concept [2]. Chelation theory suggests that the permeability of the cell wall, which is lipid-rich, allows only lipid-soluble metals to pass through. Upon chelation, the polarity of metal ions is reduced due to the overlap with ligand orbitals, which increases the lipophilicity of the complex. This enhanced lipophilicity facilitates the permeation of the complex into the lipid membrane, inhibiting protein synthesis and nucleic acid functions [4,43-44].

Burns Healing Effect of $[Zn(AH)Cl_2] \cdot H_2O$

Burns are a leading cause of death in children and a common issue within health organizations, as indicated by global epidemiological studies. Burns cause tissue destruction and necrosis through mechanisms such as destabilization of the cell membrane, protein coagulation, depletion of energy supplies, and cellular hypoxia. They also pose significant risks to other body parts when subjected to traumatic events, antigen challenges, and infectious agents. Wound healing is a crucial biological response for repairing damaged connective and epithelial tissues [2,4,19].

The burn healing efficacy of $[Zn(AH)Cl_2] \cdot H_2O$ was evaluated to determine its anti-inflammatory activity. The effectiveness of $[Zn(AH)Cl_2] \cdot H_2O$ at 1.5 mM was assessed by measuring the number of days required for recovery, with silver sulfadiazine as a positive control and an untreated group as a negative control. The results, displayed in Table 9, showed that $[Zn(AH)Cl_2] \cdot H_2O$ facilitated burn healing in 14 days, compared to 16 days for silver sulfadiazine and 18 days for the negative control. Healing was achieved without side effects, bleeding, fever, adhesion to the wound, or microbial contamination. The enhanced anti-inflammatory activity of the selected complexes is attributed to the presence of zinc ions and hypoxanthine, which contain heterocyclic rings known for their effective anti-inflammatory properties [45-46].

Realization of Radical Scavenging Performance

The *in vitro* antioxidant activity of the AH ligand was assessed using a radical scavenging technique with

Table 9. Treatments and period of recovery

No	Treatment	Period of recovery (days)
1	$[Zn(AH)Cl_2] \cdot H_2O$	14
2	Silver sulfadiazine	16
3	Without any treatment	18

Table 8. AH ligand and their complexes inhibition zone against 3 types of bacteria

Compound	*Staphylococcus aureus*	*Klebsiella pneumonia*	*Candida albicans*
Amoxicillin	20	10	-
Fluconazole	-	-	20
AH ligand	12	13	13
$[Ag(AH)(H_2O)_2]NO_3 \cdot 2H_2O$	26	12	22
$[Cu(AH)_2Cl_2] \cdot H_2O$	23	17	21
$[Zn(AH)Cl_2] \cdot H_2O$	19	14	17

Table 10. DPPH radical scavenging performance of AH ligand and vitamin C

Concentration (mg/mL)	DPPH radical scavenging activity (mean ± SD, %)	
	AH	Vitamin C
12.5	34.00 ± 1.075	42.20 ± 1.408
25	36.00 ± 1.530	57.91 ± 3.423
50	39.00 ± 1.917	65.20 ± 2.567
100	63.20 ± 2.067	78.67 ± 1.850
200	64.93 ± 2.790	85.03 ± 0.598

DPPH. Ascorbic acid was used as the positive control [2], providing a benchmark for reducing capacity. The AH ligand demonstrated greater antioxidant effectiveness compared to vitamin C at 5 concentrations: 12.5, 25, 50, 100, and 200 mg/mL [31-32]. At a concentration of 25 mg/mL, the AH ligand exhibited a DPPH radical scavenging activity of 36.00 ± 1.53%. This activity increased significantly to 64.93 ± 2.79% at 200 mg/mL (see Table 10) [28].

CONCLUSION

This study prepared and analyzed three new nano complexes derived from mono azo hypoxanthine using various spectroscopic, physicochemical, and thermal techniques. The AH ligand was found to act as a neutral *N,N*-bidentate ligand with a 1:1 (M:L) ratio when coordinated with silver and zinc ions, exhibiting tetrahedral geometry, while a 1:2 ratio with copper ions resulted in a distorted octahedral structure. The synthesized ligand and its complexes demonstrated high effectiveness against two types of bacteria and fungi, as well as notable antioxidant activity compared to ascorbic acid. The Zn-AH complex exhibited superior anti-burn and wound-healing properties compared to the standard silver sulfadiazine, as evidenced by the number of healing days. Future work will explore the detailed mechanisms of action and optimize the therapeutic applications of these newly synthesized complexes, which are potential candidates for advancement in medical and industrial fields.

ACKNOWLEDGMENTS

CONFLICT OF INTEREST

There are no conflicts of interest.

AUTHOR CONTRIBUTIONS

Alyaa Khider Abbas and Asmaa Edrees Fadhil contributed in suggesting the research design, conducting the experimental work, interpreting the results, and drafting the manuscript. All authors reviewed and approved the final version of the manuscript.

REFERENCES

[1] Crespi, S., Simeth, N.A., and König, B., 2019, Heteroaryl azo dyes as molecular photoswitches, *Nat. Rev. Chem.*, 3 (3), 133–146.

[2] Akram, D., Elhaty, I.A., and AlNeyadi, S.S., 2020, Synthesis and antibacterial activity of rhodanine-based azo dyes and their use as spectrophotometric chemosensor for Fe^{3+} ions, *Chemosensors*, 8 (16), 16.

[3] Hussein, N.A., and Abbas, A.K., 2022, Synthesis, spectroscopic characterization and thermal study of some transition metal complexes derived from caffeine azo ligand with some of their applications, *Eurasian Chem. Commun.*, 4 (1), 67–93.

[4] Jasim, D.J., and Abbas, A.K., 2022, Synthesis, identification, antibacterial, medical and dying performance studies for azo-sulfamethoxazole metal complexes, *Eurasian Chem. Commun.*, 4 (1), 16–40.

[5] Hessoon, H.M., and Abbas, H.M., 2024, Synthesis and characterization of a novel dapsone-derived bisazo ligand and its gold(III) complex, with evaluation of its antioxidant and anticancer activities, *Indones. J. Chem.*, 24 (2), 481–491.

Indones. J. Chem., xxxx, xx (x), xx - xx

11

[6] Merino, E., 2011, Synthesis of azobenzenes: The coloured pieces of molecular materials, *Chem. Soc. Rev.*, 40 (7), 3835–3853.

[7] Fadhil, A.E., and Abbas, A.K., 2023, Synthesis and structural views on new azo ligand and its metal complexes with some of their application, *Iraqi Iraqi J. Sci.*, 64 (12), 6119–6134.

[8] Toledo-Ibelles, P., Gutiérrez-Vidal, R., Calixto-Tlacomulco, S., Delgado-Coello, B., and Mas-Oliva, J., 2021, Hepatic accumulation of hypoxanthine: A link between hyperuricemia and nonalcoholic fatty liver disease, *Arch. Med. Res.*, 52 (7), 692–702.

[9] Furuhashi, M., Koyama, M., Higashiura, Y., Murase, T., Nakamura, T., Matsumoto, M., Sakai, A., Ohnishi, H., Tanaka, M., Saitoh, S., Moniwa, N., Shimamoto, K., and Miura, T., 2020, Differential regulation of hypoxanthine and xanthine by obesity in a general population, *J. Diabetes Invest.*, 11 (4), 878–887.

[10] Al-Assafe, A.Y., and Al-Quaba, R.A.M.S., 2024, New series of Ni(II), Cu(II), Zr(IV), Ag(I), and Cd(II) complexes of trimethoprim and diamine ligands: Synthesis, characterization, and biological studies, *Indones. J. Chem.*, 24 (3), 812–821.

[11] Benkhaya, S., M'rabet, S., and El Harfi, A., 2020, Classifications, properties, recent synthesis and applications of azo dyes, *Heliyon*, 6 (1), e03271.

[12] Meyer Jr., A.S., and Ayres, G.H., 1957, The mole ratio method for spectrophotometric determination of complexes in solution, *J. Am. Chem. Soc.*, 79 (1), 49–53.

[13] Volman, D.H., 1987, Gibbs energy and equilibrium: Dimensions in the Lewis equation, *Thermochim. Acta*, 111, 321–324.

[14] Khaleel, A.M.N., and Jaafar, M.I., 2017, Synthesis and characterization of boron and 2-aminophenol Schiff base ligands with their Cu(II) and Pt(IV) complexes and evaluation as antimicrobial agents, *Orient. J. Chem.*, 33 (5), 2394–2404.

[15] Al-Daffay, R.K.H., and Al-Hamdani, A.A.S., 2023, Synthesis, characterization, and thermal analysis of a new acidicazo ligand's metal complexes, *Baghdad Sci. J.*, 20 (1), 0121.

[16] Masoud, M.S., Ali, A.E., Elasala, G.S., and Kolkaila, S.A., 2017, Spectroscopic studies and thermal analysis on cefoperazone metal complexes, *J. Chem. Pharm. Res.*, 9 (4), 171–179.

[17] Patel, K.D., and Patel, H.S., 2017, Synthesis, spectroscopic characterization and thermal studies of some divalent transition metal complexes of 8-hydroxyquinoline, *Arabian J. Chem.*, 10, S1328–S1335.

[18] Hussein, K.A., Shaalan, N., Lafta, A.K., and Al Akeedi, J.M., 2024, Preparation, characterization, and biological activity of La(III), Nd(III), Er(III), Gd(III), and Dy(III) complexes with Schiff base resulted from reaction of 4-antipyrinecarboxaldehyde and 2-aminobenzothiazole, *Indones. J. Chem.*, 24 (2), 258–369.

[19] Abd, Z.Z., and Abbas, A.K., 2024, Metal complexes of adenine azo ligand: Synthesis, identification and study some of their applications, *Iraqi J. Sci.*, 65 (3), 1212–1229.

[20] Mahmoud, W.A., Ali, A.A.M., and Kareem, T.A., 2015, Preparation and spectral characterization of new azo imidazole ligand 2-[(2`-cyano phenyl) azo]-4,5-diphenyl imidazole and its complexes with Co(II), Ni(II), Cu(II), Zn(II), Cd(II) and Hg (II) ions, *Baghdad Sci. J.*, 12 (1), 96–109.

[21] Abbas, A.K., Kadhim, R.S., Khedher, R., and Latif, H.B., 2019, Synthesis, spectral and antibacterial studies of new 1-(4-Antipyrine azo)-2-hydroxy-3, 6-disulphonic acid sodium salt with group IIB metal ions, *J. Global Pharma Technol.*, 11 (4), 375–382.

[22] Abbas, A.K., and Kadhim, R.S., 2017, Metal complexes of proline-azo dyes, synthesis, characterization, dying performance and antibacterial activity studies, *Orient. J. Chem.*, 33 (1), 402–417.

[23] Hasan Mubark, H.M., Witwit, I.N., and Ali, A.A.M., 2020, Synthesis of new azo imidazole ligand and fabricating it's chelate complexes with some metallic ions, *J. Phys.: Conf. Ser.*, 1660 (1), 012031.

[24] Purwono, B., Anwar, C., and Hanapi, A., 2013, Syntheses of azo-imine derivatives from vanillin,

Indones. J. Chem., 13 (1), 1–6.

[25] Abbas, A.K., and AL-Qaysi, W.W., 2023, Synthesis and characterization of novel nano azo compounds as a new pH sensor, *Arabian J. Sci. Eng.*, 48 (1), 399–415.

[26] Shafeeulla, M., Krishnamurthy, G., Bhojynaik, H.S., and Manjuraj, T., 2017, Synthesis, cytotoxicity, and molecular docking study of complexes containing thiazole moiety, *J. Turk. Chem. Soc., Sect. A*, 4 (3), 787–810.

[27] Shaker, I.M., Salih, H.A., and Mahdi, S.M., 2016, Preparation and identification of new azo (methyl-xanthine) ligands and their transition metal complexes, *Int. J. ChemTech Res.*, 9 (10), 99–110.

[28] Abbas, N.F., and Abbas, A.K., 2020, Novel complexes of thiobarbituric acid-azo dye: Structural, spectroscopic, biological activity and dying, *Biochem. Cell. Arch.*, 20 (1), 2419–2433.

[29] Mahmoud, S.S., and Khaleel, A.M.N., 2023, Synthesis, identification and biological study of new pharmaceutical model based on amino acids with some of its complexes, *Iraqi J. Sci.*, 64 (11) 5501–5516.

[30] Al-Hamdani, A.A.S., and Abdulridha, M.Q., 2023, Synthesis, characterization of new metal complexes of Co(II), Cu(II), Cd(II) and Ru(III) from azo ligand 5-((2-(1*H*-indol-2-yl)ethyl) diazinyl)-2-aminophenol, thermal and antioxidant studies, *Baghdad Sci. J.*, 20 (Suppl. 5), 1964–1975.

[31] AL-Qaysi, W.W., and Abbas, A.K., 2023, Novel nano Zn^{+2}-compound from LA ligand as an acid-base indicator: Synthesis, characterization, pH sensor, and fluorescent study, *Iraqi J. Sci.*, 64 (11), 5525–5540.

[32] Ali, A.A., Al-Hassani, R.M., Hussain, D.H., Rheima, A.M., and Meteab, H.S., 2020, Synthesis, spectroscopic, characterization, pharmacological evaluation, and cytotoxicity assays of novel nano and micro scale of copper(II) complexes against human breast cancer cells, *Drug Invent. Today*, 14 (1), 31–39.

[33] Zolnhofer, E.M., Wijeratne, G.B., Jackson, T.A., Fortier, S., Heinemann, F.W., Meyer, K., Krzystek, J., Ozarowski, A., Mindiola, D.J., and Telser, J., 2020, Electronic structure and magnetic properties of a titanium(II) coordination complex, *Inorg. Chem.*, 59 (9), 6187–6201.

[34] Lađarević, J., Radovanović, L., Božić, B., Mašulović, A., Lunić, T., Radovanović, Ž., Rogan, J., and Mijin, D., 2023, New copper(II) complexes derived from azo pyridone dyes: Structure characterization, thermal properties, and molecular docking studies, *Appl. Organomet. Chem.*, 37 (10), e7219.

[35] Emam, S.M., Abou EL-Enein, S.A., and Monir, E., 2017, Spectrochemical and thermal sudies for bivalent metal complexes of azodye ligand containing pyrimidine ring, *Int. J. Eng. Res. Sci. Technol.*, 6 (9), 354–364.

[36] Kurutos, A., Kamounah, F.S., Dobrikov, G.M., Pittelkow, M., Sauer, S.P.A., and Hansen, P.E., 2021, Azo-hydrazone molecular switches: Synthesis and NMR conformational investigation, *Magn. Reson. Chem.*, 59 (11), 1116–1125.

[37] Qazi, S.J.S., Rennie, A.R., Cockcroft, J.K., and Vickers, M., 2009, Use of wide-angle X-ray diffraction to measure shape and size of dispersed colloidal particles, *J. Colloid Interface Sci.*, 338 (1), 105–110.

[38] Bragg, W.H., and Bragg, W.L., 1913, The reflection of X-rays by crystals, *Proc. R. Soc. A*, 88 (605), 428–438

[39] Humphreys, C.J., 2013, The significance of Bragg's law in electron diffraction and microscopy, and Bragg's second law, *Acta Crystallogr., Sect. A: Found. Adv.*, 69 (1), 45–50.

[40] Greenberg, B., 1989, Bragg's law with refraction, *Acta Crystallogr., Sect. A: Found. Adv.*, 45 (3), 238–241.

[41] Ghomrasni, N.B., Chivas-Joly, C., Devoille, L., Hochepied, J.F., and Feltin, N., 2020, Challenges in sample preparation for measuring nanoparticles size by scanning electron microscopy from suspensions, powder form and complex media, *Powder Technol.*, 359, 226–237.

[42] Elsayed, E.H., Al-Wahaib, D., Ali, A.E.D., Abd-El-Nabey, B.A., and Elbadawy, H.A., 2023, Synthesis, characterization, DNA binding interactions, DFT calculations, and Covid-19 molecular docking of novel bioactive copper(I) complexes developed via unexpected reduction of azo-hydrazo ligands, *BMC Chem.*, 17 (1), 159.

[43] AbdulRazzaq, A.B., Shami, A.M., and Ghaima, K.K., 2022, Detection of *vanA* and *vanB* genes among vancomycin resistant *Staphylococcus aureus* isolated from clinical samples in Baghdad hospitals, *Iraqi J. Biotechnol.*, 21 (1), 19–25.

[44] Al-Hayali, O.Z., AL Marjani, M.F., and Maleki, A., 2023, Evaluation of *Rosmarinus officinalis* leaves essential oils activity against vancomycin intermediate *Staphylococcus aureus* (VISA) isolated from Baghdad hospital patients, *Iraqi J. Sci.*, 64 (5), 2153–2167.

[45] Kumar, A., Sharma, P., and Sharma, P.K., 2017, Exploration of antioxidant activity of newly synthesized azo flavones and its correlation with electrochemical parameters along with the study of their redox behaviour, *J. Anal. Chem.*, 72 (10), 1034–1044.

[46] Lestari, T., Syukur, S., Revilla, G., Rita, R.S., and Rustini, R., 2023, The burn wound healing process: A review, *Int. J. Prog. Sci. Technol.*, 40 (1), 77–88.